Waste Management 177 (2024) 135–145

Contents lists available at ScienceDirect

Waste Management

journal homepage: www.elsevier.com/locate/wasman

Research Paper

Exploring the insights and benefits of biomass-derived sulfuric acid activated carbon for selective recovery of gold from simulated waste streams

John Kwame Bediako [a,b,*], Enoch Kudoahor [c], Che-Ryong Lim [d], Nicole Sharon Affrifah [b], Sok Kim [e], Myung-Hee Song [d], Eveliina Repo [a]

[a] Department of Separation Science, School of Engineering Science, Lappeenranta-Lahti University of Technology (LUT), FI-53850, Lappeenranta, Finland
[b] Department of Food Process Engineering, School of Engineering Sciences, College of Basic and Applied Sciences, University of Ghana, P. O. Box LG 77, Legon, Accra, Ghana
[c] Department of Chemistry and Biochemistry, University of Arkansas, Fayetteville, AR 72701, USA
[d] Division of Semiconductor and Chemical Engineering, Jeonbuk National University, Jeonju, Jeonbuk 561-756, Republic of Korea
[e] Division of Environmental Science & Ecological Engineering, Korea University, Seoul 02841, Republic of Korea

ARTICLE INFO

Keywords:
Selective gold recovery
H_2SO_4-AC
Agro-waste biomass
E-waste
DFT computation

ABSTRACT

The surging affluent in society, concomitant with increasing global demand for electrical and electronic devices, has led to a sharp rise in e-waste generation. E-wastes contain significant amounts of precious metals, such as gold, which can be recovered and reused, thus reducing the environmental impact of mining new metals. Selective recovery using sustainable and cost-effective materials and methods is therefore vital. This study undertook a detailed evaluation of low-cost biomass-derived activated carbon (AC) for selective recovery of Au from simulated e-waste streams. Utilizing high-performance synthesized H_2SO_4-AC, the adsorption mechanisms were explicated through a combination of characterization techniques, i.e., FE-SEM, BET, TGA, XRD, FTIR, XPS, and DFT simulations to conceptualize the atomic and molecular level interactions. Optimization of coordination geometries between model H_2SO_4-AC and anionic complexes revealed the most stable coordination for $AuCl_4^-$ (binding energy, E_b = -4064.15 eV). The Au selectivity was further enhanced by reduction of Au(III) to Au(0), as determined by XRD and XPS. The adsorption reaction was relatively fast (~5h), and maximum Au uptake reached 1679.74 ± 37.66 mg/g (among highest), achieved through adsorption isotherm experiments. Furthermore, a mixture of 0.5 M thiourea/1 M HCl could effectively elute the loaded Au and regenerate the spent AC. This study presents radical attempts to examine in detail, the synergistic effects of H_2SO_4 activation on biomass-derived ACs for selective recovery of Au from complex mixtures. The paper therefore describes a novel approach for the selective recovery of Au from e-wastes using multifunctional biomass-derived H_2SO_4-AC.

1. Introduction

The indiscriminate disposal of electrical and electronic wastes (e-wastes) has become a major environmental concern due to the potential release of hazardous materials, including precious metals, e.g., Au, Pt, and Pd into the environment (Chand et al., 2009; Changmei et al., 2011; Lin et al., 2017; Mao et al., 2015). Particularly, Au is a valuable metal that is commonly used in many devices, and its recovery from e-wastes has the possibility to not only reduce environmental pollution but also provide a sustainable source of supply to industries (Chand et al., 2009; Bediako et al., 2023). This will also secure the depleting natural reserves and lessen the environmental impact of mining from primary ores (Chand et al., 2009; Changmei et al., 2011; Lin et al., 2017; Mao et al., 2015). Gold finds extensive application in the coinage, jewelry, electronic, automobile, electroplating and medical fields (Chand et al., 2009; Changmei et al., 2011; Erim et al., 2013; Bediako et al., 2023; Lin et al., 2017; Ramesh et al., 2008). It upholds a special economic importance in its long-standing history as a traded currency for transactions and also as an investment commodity (Changmei et al., 2011; Erim et al., 2013). In the past, the spent gadgets or devices containing Au were usually disposed of unrecycled, which led to resource wastages and public health hazards. However, global rising concerns over the

* Corresponding author.
E-mail address: john.bediako@lut.fi (J.K. Bediako).

https://doi.org/10.1016/j.wasman.2024.02.002
Received 25 August 2023; Received in revised form 6 January 2024; Accepted 2 February 2024
Available online 6 February 2024

continuous deterioration of the fewer available natural ore reserves have inspired the need for recycling these e-wastes in order to recover the precious minerals (Bediako et al., 2023; Lin et al., 2017).

Technologies including adsorption, solvent extraction, co-precipitation, reverse osmosis, and electrocoagulation are widely applied (Bediako et al., 2023; Changmei et al., 2011; Bediako et al., 2023). Comparatively, the liquid–liquid extraction technique is mostly useful owing to its high loading capacity and fast extraction rate; however, it is less effective at dilute metal concentrations, and the fact that it faces mixing, settlement, and solvent loss problems also limit its full application potentials (Changmei et al., 2011; Iglesias et al., 1999; Bediako et al., 2023; Wei et al., 2016c). Adsorption as a type of solid–liquid interface technique is suitable even in the case of very low metal concentrations and permits selective separation of target metals from interfering metals. Therefore, it is considered as one of the most effective methods to recover Au from complex solutions, such as acid-leached e-wastes (Changmei et al., 2011; Fujiwara et al., 2007; Iglesias et al., 1999).

A wide range of adsorbents, including activated carbon (AC), ion-exchange resins, microbial waste materials, mesoporous and polymer-based adsorbents have been developed and investigated (Awual et al., 2013; Dodson et al., 2015; Lam et al., 2006; Li et al., 2015; Park et al., 2012; Qu et al., 2009). However, while most microbial and polymer-based adsorbents cannot withstand the harsh conditions of the classical lixiviation process which mostly employs aqua regia, doped mesoporous adsorbents suffer from instability as most of the connecting linkages are non-covalently held and tend to break apart during the adsorption process (Bediako et al., 2019; Bediako et al., 2023). This instability may lead to leaching of toxic chemicals into the adsorption media thereby causing unwanted secondary pollutions, the treatments of which could lead to extra processing costs (Bediako et al., 2019; Bediako et al., 2023). On the other hand, ion-exchange resins can effectively function in a wide range of pH, including acidic regions (Chand et al., 2009; El Ouardi et al., 2023); however, incineration of the plastic resins to recover the reduced metallic Au is cumbersome and energy-consuming (Chand et al., 2009).

Thus, AC remains the single most effective and economically preferred option in the conventional Au recovery processes owing to its good stability, high specific surface area, and pore volume, leading to high uptakes and fast adsorption rates (Adams et al., 2020; Chand et al., 2009; Soleimani and Kaghazchi, 2008a, b). In recent times, researchers have been exploiting cheaper and readily abundant carbon precursors to replace the expensive commercial carbons (El Ouardi et al., 2022; Soleimani and Kaghazchi, 2008a, b). In this regard, the types of raw materials and activation protocols are observed to have direct impacts on the textural and chemical characteristics of the synthesized ACs, such as surface area formation, porosity development, and surface reactivity of the ACs (Bedin et al., 2016; Chand et al., 2009; Unur, 2013). In this study, we investigated the synergistic effects of carbon precursors and activation agents on Au recovery efficiencies of ACs synthesized from selected agro-waste biomasses. By expounding the underlying mechanisms through instrumental characterization and computational probes, we identified some intriguing effects of H_2SO_4 activation, such as the introduction of strong-affinity N, O and S-containing groups that triggered high Au selectivity. Ordinarily, introduction of these heteroatoms onto the surface of AC for improved functionality require long complicated methods (Yang et al., 2019). As far as we are aware, this work represents a pioneering effort to comprehensively examine the combined impacts of H_2SO_4 activation on AC derived from biomass, with the aim of selectively extracting Au from complex mixtures of e-wastes; therefore, the study can serve as a helpful blueprint for further research.

2. Materials and methods

2.1. Materials and chemicals used

Agro-waste biomass precursors were received from Ghana, and include cocoa pod husk, banana peel, mango peel, orange peel, cassava peel, plantain peel, and pineapple peel. The dried samples were cleaned by washing with distilled water and oven-dried for 24 h at 70 °C. Five different reagents, including acids and bases were selected for the activation process. H_2SO_4, KOH, NaOH and HCl were obtained from Daejung Chemicals and Metals Co., Ltd. (Gyeonggi-do, South Korea). H_3PO_4 and $ZnCl_2$ were supplied by Sigma-Aldrich Korea Ltd. (Gyeonggi-do, South Korea). Model e-waste stock solution containing Au was prepared from $HAuCl_4{\cdot}3{\cdot}.7H_2O$ (Kojima Chemicals, South Korea) in 0.1 M HCl to mimic the naturally strong acidic conditions (Wei et al., 2016b). Competing metal ion stock solutions were prepared from chloro complexes of Pd and Pt, and nitrate complexes of Ag, Co, Cu, and Ni, all in 0.1 M HCl. Double distilled water (DW, Direct-Q UV Millipore dispenser, Merck Millipore) was used throughout the study for dilutions and preparation of all the solutions.

2.2. Synthesis of ACs

The clean dried biomass precursors were grounded into fine granules with the help of a Philips blender and sieved through layers of meshes. Those grains that passed through a 2 mm mesh but retained on a 0.35 mm mesh were used for the AC synthesis. Approximately 6 g of biomass samples were weighed and pre-carbonized in an automated furnace at 400 °C for 1 h under continuous N_2 supply and allowed to cool naturally to room temperature. From preliminary data (Supplementary Material, S1 and Fig. S1), the pre-carbonized orange peel (OP) precursor was selected and treated with different activation agents, i.e., H_2SO_4, H_3PO_4, KOH, NaOH and $ZnCl_2$ in a fixed ratio of 2:1 for 3 h. Next, the samples were filtered and kept in an oven dryer for ~ 24 h. The activation agent-impregnated carbonized precursors were further activated at 800 °C for 1 h under N_2 environment in the automated furnace. The obtained ACs were rinsed with DW, dried at 70 °C for ~ 24 h, and labeled according to the activation agent employed. A summary flow chart of the AC synthesis process is provided in the SI, Fig. S2.

2.3. Characterization of the ACs

2.3.1. Instrumental characterization

The pristine OP and H_2SO_4-AC (sulfuric acid-activated carbon) were characterized using field emission scanning electron microscope, FE-SEM (SUPRA 40VP, Carl Zeiss, Germany) with embedded energy dispersive X-ray spectroscope (EDX), in order to study their surface morphologies and elemental make-ups. To prevent surface charging during the analysis, Pt was used to sputter-coat the surfaces of the samples prior to analysis. Functional group analysis was done with Fourier transforms infrared (FTIR) spectrometer (PerkinElmer spectrophotometer: Spectrum GX, FTIR System). Infrared spectra of the samples were collected with KBr disks in the wavelength range from 4000 to 400 cm^{-1}. Thermal profiles were recorded using a thermal analyzer (TA Q600 DSC/TGA, TA Instruments, USA) with maximum operating temperature of up to 1000 °C. The crystallinities were analyzed using X-ray diffractometer, XRD (multi-purpose high-performance X-ray diffractometer, X'pert Powder, PANalytical, the Netherlands) with a Cu-Kα radiation operating at 40 kV and 30 mA at a scan rate of 10° min^{-1} in the 2θ range of 5° to 80°. Nitrogen gas (N_2) adsorption isotherm measurements were run on a BELSORP-max BET equipment at 77 K. The samples were activated by heating at 100 °C for 12 h under high vacuum. Density functional theory (DFT) model embedded in the BET equipment was used to calculate the pore size distributions. Moreover, the atomic bonding and valence states of C, N, O, S, Cl, and Au were analyzed using X-ray photoelectron spectroscopy, XPS equipment (AXIS-NOVA

spectrometer, Kratos Analytical, Ltd., UK) with monochromatic Al Kα as the X-ray source (1486.71 eV of photons). Furthermore, the pH point of zero charge, pH_{pzc} of the H_2SO_4-AC was measured following the pH drift method described elsewhere (Sarkar et al., 2019; Wei et al., 2016c).

2.3.2. DFT computations

Molecular and energy computations were carried out using Spartan'20 Parallel Suite QC program (Spartan'20® version 1.1.4, Wavefunction, Inc., 18,401 Von Karman Ave., Suite 370 Irvine, CA 92612, U.S.A., 2022). To simulate a molecular configuration of the synthesized H_2SO_4-AC, a slab of carbon bearing 10 aromatic rings and a total of 31 carbon atoms was used as the base carbon material (Bacirhonde et al., 2022). Following data from the characterization, particularly XPS, it was understood that the H_2SO_4-AC possesses different kinds of N, O, and S groups. Based on this knowledge, the H_2SO_4-AC was modeled by etching these atoms into the carbon slab and then optimized. The structure was first drawn using ChemDraw® (version 17.1.0.105(19), PerkinElmer Informatics, Inc. © 1998–2018) and then exported to the Spartan'20 software for the DFT calculations. To ensure uniformity, the optimized structure was used to simulate the binding energies between the H_2SO_4-AC and anionic metal complexes. In this work, the Becke-three-Lee–Yang–Parr (B3LYP) method, a 6-31G* and LANL2DZ > Kr basic set were used for each complex at the ground state, and water was used as the solvent (Shao et al., 2015). Total charges for each complex were inputted and the Spartan'20 software was used to obtain the energy for each complex through DFT computations.

2.4. Adsorption studies

2.4.1. Preliminary adsorption experiments

The stock solutions were first diluted into working solutions to undertake the adsorption experiments. Initial adsorption evaluations were performed using the different precursor- and activation agent-based ACs in comparison to the pristine biomasses. About 0.02 g ACs were weighed into 50 mL falcon bottles and 30 mL of metal solutions were added and placed in a multi-shaking incubator at 25 ± 2 °C and 140 rpm for 24 h. To analyze the adsorbed samples, the solutions were centrifuged to obtain clear supernatants. These supernatants were then appropriately diluted and subjected to analysis using an inductively coupled plasma-atomic emission spectrometer (Thermo Scientific, iCAP 7000 series, ICP Spectrometer, USA). The resulting data were processed in MS Excel and the metal uptakes were estimated using the mass balance expression in Eq. (1).

$$q = \frac{(C_i - C_e)V}{M} \tag{1}$$

where C_i and C_e are initial and equilibrium concentrations in mg/L, V is the volume in L, and M is dry mass of AC in g.

2.4.2. Adsorption isotherms and competing metal adsorption

The same adsorbent dosage, i.e., 0.02 g/30 mL used for the preliminary adsorption experiments was applied in the adsorption isotherm experiments; however, the initial metal concentrations were varied from 0 to 2000 mg/L. Here again, the samples were placed in a multi-shaking incubator kept at 25 ± 2 °C and 140 rpm for 24 h. Furthermore, the effects of competing ions were performed at different concentrations using the same adsorbent dosage and experimental conditions. The adsorption data were treated in SigmaPlot software (version 12.0, SPSS, USA) and fitted through the Langmuir (Langmuir, 1918) and Freundlich (Freundlich, 1906) isotherm models presented in the following equations:

$$\text{Langmuir model}: \; q_e = q_m \frac{bC_e}{1 + bC_e} \tag{2}$$

$$\text{Freundlich model}: \; q_e = KC_e^{1/n} \tag{3}$$

where q_m is maximum uptake at equilibrium (mg/g), b is the coefficient relating to the affinity between the adsorbents and adsorbates, q_e is the equilibrium uptake (mg/g), C_e is the equilibrium adsorbate concentration (mg/L), K and n are the Freundlich constants denoting the relative adsorption capacity and adsorption intensity, respectively. In addition, the selectivity coefficient, Sel_i and fractional selectivity, Sel_{Fi} were calculated using Eq. (4) and Eq. (5) as expressed below.

$$Sel_i = \frac{(q_e/C_e)_i}{\sum(q_e/C_e)_j} \tag{4}$$

$$Sel_i = \frac{(q_e)_i}{\sum(q_e)_k} \tag{5}$$

where Sel_i is the selectivity coefficient of the target metal, i, which is Au in this study, j represents the competing metal ions in the solution, and k denotes both the target and competing ions (Bediako et al., 2020a; Changmei et al., 2011; Wei et al., 2016c).

2.4.3. Adsorption kinetics and adsorbent regeneration

For the kinetic experiments, ~500 mg/L initial metal concentration was used, and the adsorbent dosage was increased in a correspondingly large volume of the metal solution. That is, 0.2 g AC immersed in 500 mL metal solution was placed on multi-purpose stirring equipment with a magnetic stirring bar at ambient temperature and 300 rpm. About 1 mL of the solution was timely pipetted from the bulk phase within 0 – 24 h, centrifuged and diluted for analyses using the ICP. Here too, the adsorption data were exported to SigmaPlot and correlated through the pseudo-first-order and pseudo-second-order kinetic models (Ho and McKay, 1999; Lagergren, 1898) represented by the following expressions:

$$\text{Pseudo} - \text{first} - \text{order}: \; q_t = q_1(1 - exp(-k_1 t)) \tag{6}$$

$$\text{Pseudo} - \text{second} - \text{order}: \; q_t = \frac{q_2^2 k_2 t}{1 + q_2 k_2 t} \tag{7}$$

where q_{e1} and q_{e2} are the equilibrium uptakes (mg/g); q_t is the adsorption amount at time, t (mg/g); k_1 is the first-order equilibrium rate constant (min^{-1}), and k_2 is the second-order equilibrium rate constant (g/mg min). All other symbols are as earlier defined above. To find the best eluent for desorption and regeneration of the synthesized AC, several candidates including HNO_3, H_2SO_4, HCl, and thiourea (TU) were tested at initial Au(III) concentration of 500 mg/L. Adsorption experiments were first conducted, and then the metal loaded-ACs were separated, re-immersed into the eluent solutions and placed in the shaking-incubator maintained at 140 rpm and 25 ± 2 °C for 24 h. The metal-free ACs were rinsed with DW and the next adsorption cycle began.

3. Results and discussion

3.1. Adsorption evaluations

3.1.1. Preliminary adsorption evaluations

Adsorption capacities of the pristine biomasses and corresponding ACs are shown in Fig. S1. The activated samples showed much improved Au uptakes compared to the virgin biomass precursors. Although the biomass precursors showed substantial Au uptakes, the adsorption capacities became further enhanced after activation. The Au uptakes ranged from 422.61 to 529.30 mg/g Au, with the highest being the AC obtained from OP biomass. Based on this result, the OP was selected as a precursor to synthesize the activation agent-based ACs. It could be seen from Fig. 1 that the H_2SO_4-AC and $ZnCl_2$-AC recorded the best uptakes of 591.10 and 569.78 mg/g, respectively. Indeed, ACs synthesized through $ZnCl_2$ activation exhibit notably higher surface areas (Din et al., 2017), hence leading to high uptakes. However, evidence from safety data

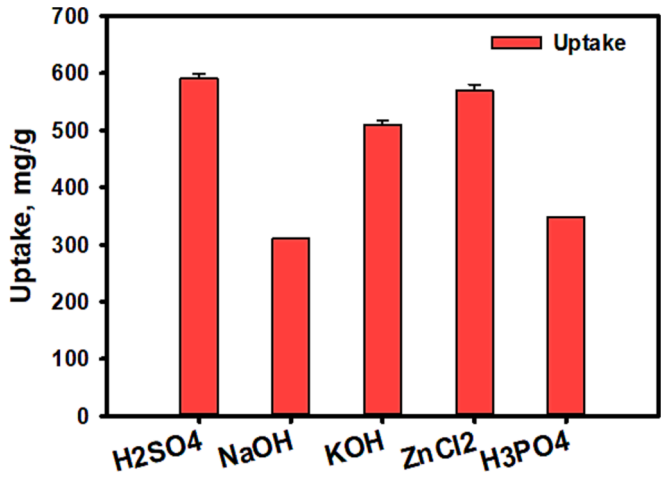

Fig. 1. Single-point adsorption evaluations of activation agent-based ACs. Experimental conditions: adsorbent dosage; 0.02 g/30 mL, initial metal conc.; ~500 mg/L, temp.; 25 ± 2 °C, rotation speed; 140 rpm, reaction time; 24 h, pH; ~1.

sheets and other reliable sources point to the fact that $ZnCl_2$ is a highly corrosive agent that can cause severe systemic toxicity, thus making it a less favorable option for further exploration. In fact, metallic oxides are generally among several factors that can cause sterner disposal guidelines for used ACs (Le-Minh et al., 2018). Aside exhibiting a slightly higher adsorption capacity, the H_2SO_4-AC was a better option owing to the extra functionality associated with H_2SO_4 activation. Heteroatoms with great affinities for binding Au are introduced onto/into the AC through H_2SO_4 activation (Le-Minh et al., 2018). Notably, the pH_{pzc} of the H_2SO_4-AC is 6.8 (Fig. S3), which means that its surface bears a neutral charge at this point, positively charged below it, and negatively charged above it (Sarkar et al., 2019; Wei et al., 2016c). Therefore, further characterization and subsequent adsorption experiments were conducted using the H_2SO_4-AC.

3.1.2. *Competitive adsorption studies*

To evaluate the selective adsorption performance of the as-synthesized H_2SO_4-AC, competitive adsorption experiments were carried out. In these experiments, the selective adsorption of Au over interfering ions was performed at low and high concentrations in Au/Pt/Pd ternary and Au/Pt/Pd/Ag/Co/Zn/Cu/Ni multiple mixtures, so as to well appreciate the competitive interactions (Fig. 2). In these complex competitive mixtures, the selectivity of Au was observed to increase marginally as the initial concentrations were changed from ~ 150 mg/L (low) to ~ 500 mg/L (high) (Fig. 2(a) and (b)). In the Au/Pt/Pd ternary system, the Sel_i values were 8.59 and 7.48. Alternatively, the Sel_{Fi} estimated the relative Au recovery efficiency as ~ 87 and 86 %. Primarily, the increase in selectivity could be first explained on the bases of concentration gradient, available binding sites and adsorption affinity (Anirudhan et al., 2012; Bediako et al., 2015; Bediako et al., 2016). As discussed later, the surface of AC is composed of many functional groups including N, O, and S groups. In an extreme acidic environment as employed in this study, the N-bearing functional groups tend to become heavily protonated, leading to considerable net positive charges on the AC surface. This is further corroborated by the pH_{pzc} being 6.8 (Fig. S3). On the other hand, the O and S-bearing groups tend to attract protons (H^+), thereby decreasing their affinity for other ions. Thus, the selective adsorption of Au in the presence of cationic metal ions is well justified. Considering concentration dependence, it could be explained that at lower concentrations, there were probably more binding sites than competing ions; as the competition became intensified at higher concentrations, a special driving force was preferentially provided in favor of Au to the detriment of the other ions, leading to high Au adsorption.

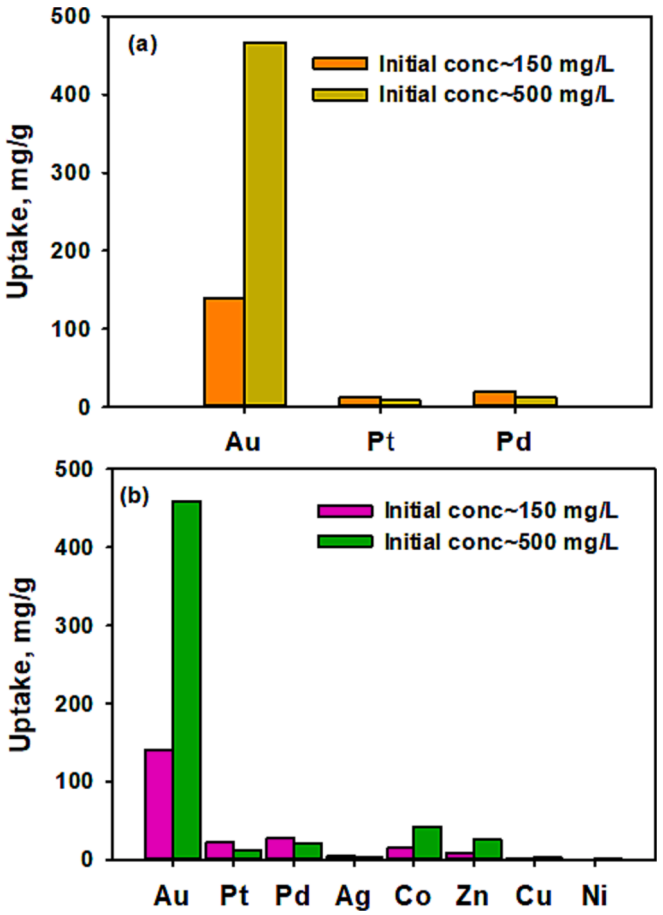

Fig. 2. Competitive adsorption studies using H_2SO_4-AC in (a) Au/Pt/Pd ternary system and (b) Au/Pt/Pd/Ag/Co/Zn/Cu/Ni multiple mixtures at ~ 150 mg/L (low) to ~ 500 mg/L (high) initial concentrations. Experimental conditions: adsorbent dosage; 0.02 g/30 mL, initial metal conc.; ~150 and ~ 500 mg/L, temp.; 25 ± 2 °C, rotation speed; 140 rpm, reaction time; 24 h, pH; ~1.

To fully elucidate the selective adsorption mechanisms, instrumental characterization and computational analysis were conducted and duly discussed subsequently.

3.2. *Characterization of the H_2SO_4-AC*

3.2.1. *FE-SEM morphology and EDX elemental analyses*

The surface morphologies and elemental peaks of the OP and H_2SO_4-AC are shown in Fig. 3. As can be seen from the FE-SEM images, the carbonized biomass became much perforated with many revealing porous structures on its surface. Noteworthily, the activation process of H_2SO_4 is said to proceed by initiation of bond cleaving, which leads to dehydration, liberation and elimination of various light and volatile substances, thereby yielding partial aromatization and hence carbonization (Khaled et al., 2009). The development of the observed porous structures on the H_2SO_4-AC surface was therefore a result of the above highlighted reactions. As is the ideal case, the porosity lessened drastically after adsorption, due to pore filling and adherence of the Au chloride complexes into the porous structures. The elemental graphs indicate high compositions of C with heteroatoms, including N, O, and S. The presence of Pt peaks is however due to the sputter-coating that was done to prevent surface charging during the measurements. Moreover, the presence of Au peak on the surface of the H_2SO_4-AC after adsorption provides initial evidence of retention of the adsorbed Au on the surface of the AC.

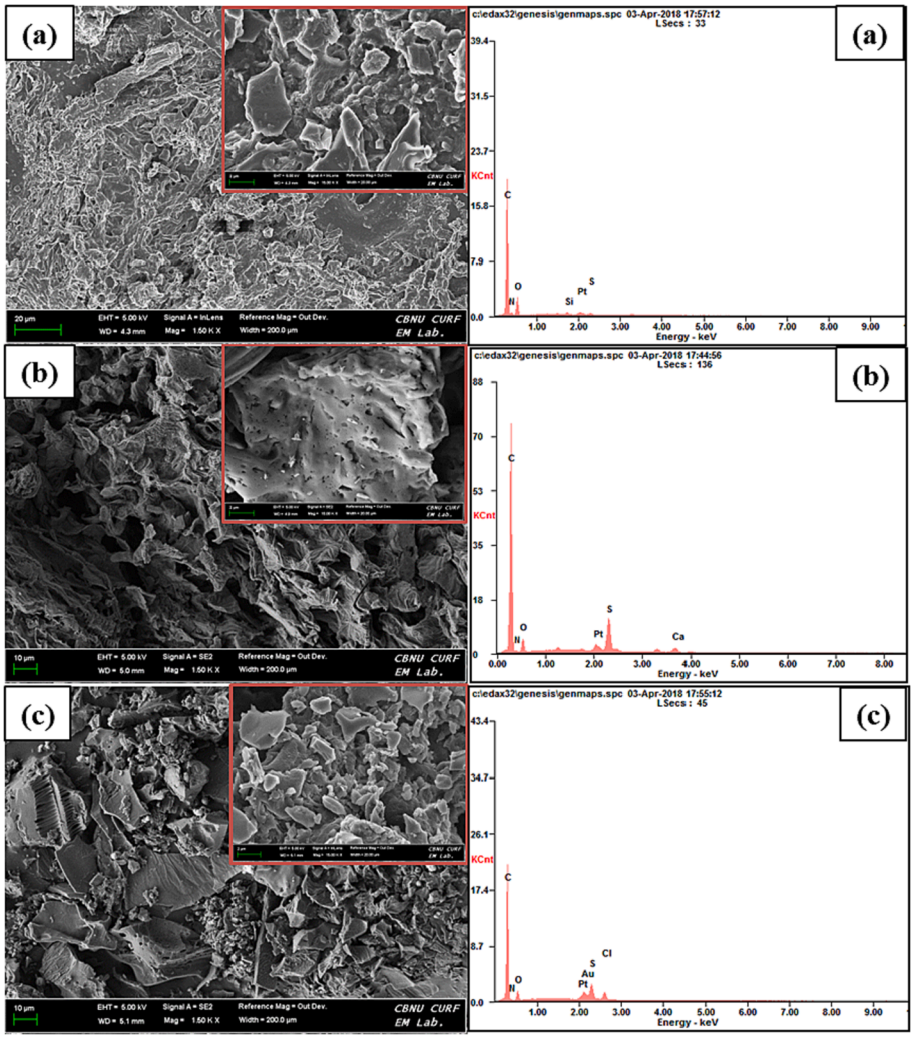

Fig. 3. FE-SEM images and EDX elemental patterns of (a) pristine OP, (b) H_2SO_4-AC and (c) gold loaded H_2SO_4-AC.

3.2.2. *FTIR, BET and TGA analyses*

Several infrared absorption peaks representing characteristic functional groups were identified before and after carbon activation (Fig. 4 (a)). The broad and high-intensity peaks at around 3452.77 cm^{-1} are suggestive of the presence of hydroxyl (O–H) and amine (N–H) groups, and the low-intensity peaks at 2958.13 and 2884.29 cm^{-1} correspond to $–CH_2$ and $–CH_3$ stretching, respectively (Guidi et al., 2012; Gupta and Nayak, 2012; Karaçetin et al., 2014; Khaled et al., 2009; Mahapatra and Ramachandra, 2013; Song et al., 2016). In addition, the peaks appearing at 1641.14 and 1429.73 cm^{-1} are due to asymmetric and symmetric C = O vibrations of carboxylic acid groups and C = C skeletal stretching in the condensed aromatic structures (Khaled et al., 2009; El Ouardi et al., 2022). The peak at 1279.82 cm^{-1} represents C-S vibration, at 1071.65 cm^{-1} corresponds to carbonyl C–O/C–O–C stretching of the polysaccharide skeleton, and at 577.16 is due to N–H out-of-plane bending and torsional vibration of the glucopyranose ring (Cortes et al., 2015; Martins et al., 2015; Wei et al., 2015; Zhou et al., 2017). Moreover, in the spectrum of the H_2SO_4-AC, C = N vibration (Elwakeel et al., 2016) and C–N stretching (Cortes et al., 2015) overlap with the C = O and C = C bonds at the region between 1641.14 and 1429.73 cm^{-1}, likely resulting from nitrogen doping into the AC structure. These indicate that the carbon activation led to increased aromaticity, decomposition and cracking of a great number of structural components of the pristine biomass (Khaled et al., 2009).

Furthermore, BET surface area and pore size distributions of the H_2SO_4-AC were measured via N_2 physical adsorption. From Fig. 4(b), it could be seen that the pristine biomass showed no adsorptive affinity for nitrogen, and hence no characteristic pore size was observed (inset figure). However, after carbon activation, a type-IV isotherm curve with a very high N_2 adsorption capacity reaching 196.38 cm^3 (STP)/g, surface area of 1211.22 m^2/g and two types of micropores at *ca.* 0.7 and 1.3 nm are clearly visible. Besides, the TGA thermal stability of the activated sample improved much significantly from an initial weight loss of > 70 % in the pristine OP to just about only 15 % in the H_2SO_4-AC (Fig. 4(c)). The textural and thermal properties thus well complement the observations made from the morphological studies.

3.3. *Investigation of the selective adsorption mechanisms*

3.3.1. *DFT computations using Spartan® software*

To examine the mechanisms leading to Au selectivity in the presence of competing ions, DFT computations were run using the Spartan'20 software. To begin with, optimized model structure of the as-synthesized H_2SO_4-AC was generated based on the instrumental characterizations, including XPS deconvoluted results of the N, O and S atoms (discussed later). Next, all required parameters were set and the DFT calculations were run to obtain the optimal coordination geometries between the configured H_2SO_4-AC and anionic metal complexes of Au, Pd and Pt (Fig. S4). After that, the binding energies, E_b between the H_2SO_4-AC and each of the three metal complexes were independently determined based on their optimized coordination modes. The optimization provided the lowest energy possible for molecular interaction, whilst the

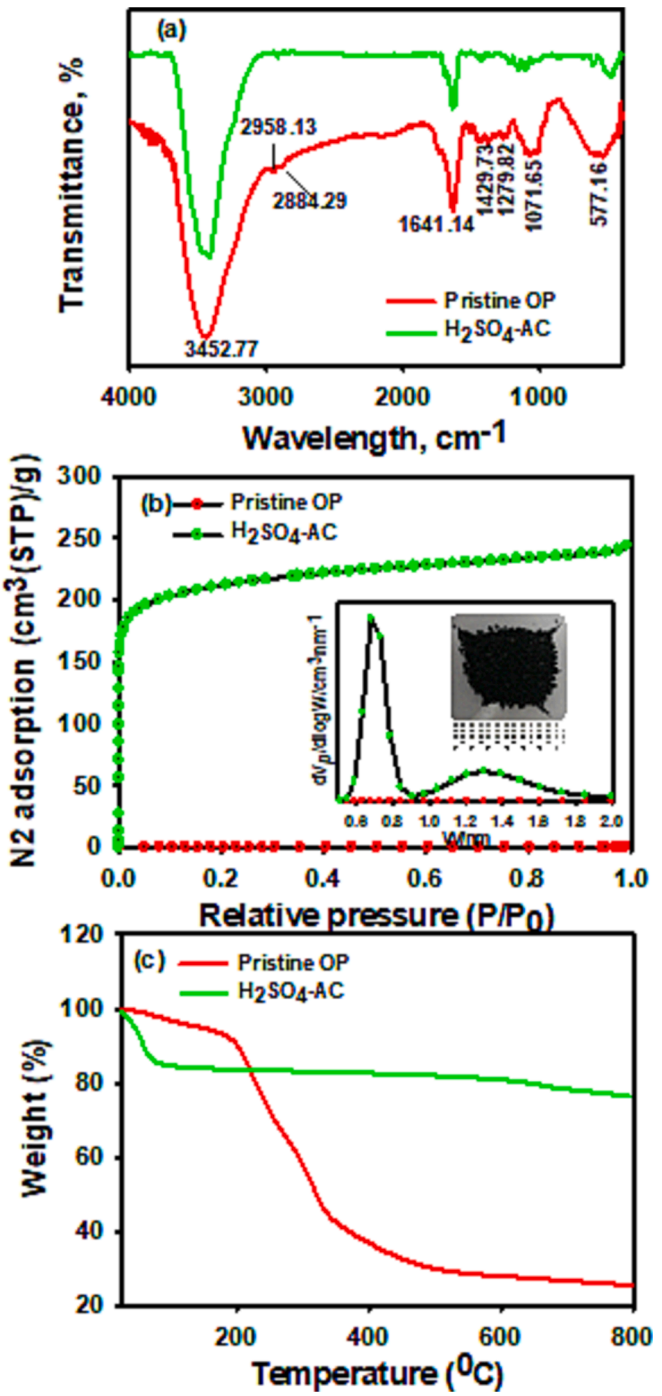

Fig. 4. (a) FTIR functional group, (b) BET textural properties and (c) TGA thermal profiles.

energy calculations gave the E_b of the interacting species at their ground state in solution (Shao et al., 2015; Bacirhonde et al., 2022).

Molecular electron potential (ESP) energy surfaces deduced from the interactions between the optimized H_2SO_4-AC structure and the anionic metal complexes with corresponding E_b are shown in Fig. 5. According to literature, the most predominant forms of these metals in aqueous solution are $AuCl_4^-$, $PdCl_4^{2-}$, $PtCl_4^{2-}$ and $PtCl_6^{2-}$ (Won et al., 2014; Bediako et al., 2019; Karhu et al., 2003; Wei et al., 2016a). The calculated E_b are in the order of $PtCl_6^{2-}$ (-4968.51 eV) > $AuCl_4^-$ (-4064.15 eV) > $PdCl_4^{2-}$ (-4055.70 eV) > $PtCl_4^{2-}$ (-4048.12 eV). Although $PtCl_6^{2-}$ displayed the highest binding energy (most stable coordination), suggesting that a stronger driving force might be pulling it towards the AC, the co-existence of both $PtCl_6^{2-}$ and $PtCl_4^{2-}$ species in the solution might have hindered the actual amount of $PtCl_6^{2-}$ bound at equilibrium. Hence, it is interesting to observe a rather high selectivity of the H_2SO_4-AC towards $AuCl_4^-$. Besides, the average sizes of the AC micropores, coupled with the observed reduction reactions tend to favor Au capture. The above discussion gives substantial appreciation of the selective adsorption of $AuCl_4^-$. The succeeding section provides further support for the specific adsorption (reaction) pathways and mechanisms leading to the Au selectivity.

3.3.2. XRD and XPS analyses

To further probe the selective adsorption mechanisms, XRD and XPS analysis were undertaken. XRD crystalline patterns and XPS deconvoluted spectra of the OP and H_2SO_4-AC are shown in Fig. 6 and Fig. S5 – S7. In addition, chemical compositions in the form of atomic weight percentages of different elemental scans for the pristine biomass and AC samples are presented in Table S1. In Fig. 6(a), two low-intensity broad peaks appeared at the 2θ values of 15.9 and 21.6°, which could be assigned to the crystalline glycosidic units of the cellulose structure in the pristine biomass (Bediako et al., 2015; Zhang et al., 2018). Conversely, the H_2SO_4-AC displayed a characteristic graphite-like reflection of the (002) plane at approximately $2\theta = 24.1°$, with corresponding weak amorphous-like peaks at 27.1, 31.0 and 43.2°, signifying the mixed presence of both ordered and non-ordered graphitized structures (Chen et al., 2010; Huang et al., 2011). In the case of the Au-loaded H_2SO_4-AC, high-intensity diffraction peaks at the 2θ values of 37.9, 44.2, 64.4 and 77.6°, corresponding to the (111), (200), (220) and (311) lattice planes of crystalline Au nanoparticles were observed (Bediako et al., 2017; Zhang et al., 2018). These peaks pointed to the formation of face centered cubic (fcc) crystalline structures of zero-valent Au nanoparticles, and thus indicated reduction of ionic Au(III) to solid Au(0) (Bediako et al., 2017; Park et al., 2013). In addition, the (111) plane showed the highest intensity, thus suggesting that it presented the most dominant orientation of the reduced Au nanoparticles (Kanmani and Rhim, 2014; Zhao et al., 2015).

The presence of reduced and non-reduced Au was further revealed by the high-resolution core-level Au4f spectrum of the Au-loaded H_2SO_4-AC, indicating that a significant portion of the adsorbed Au was retained in its chloro-Au complex form of $AuCl_4^-$ (Fig. 6(b)). This was further justified by the pairs of Cl2p peaks shown in Fig. 6(c) and (d). In other words, the peak pair of $Cl2p_{3/2}$ and $Cl2p_{1/2}$ established at 198.08 and 199.68 eV, respectively, is traced to adhering organic chlorine on the surface of the biomass, and those at 200.00 and 201.16 eV belong to the Cl^- from the adsorbed chloro-Au complex (Dong et al., 2011; Wei et al., 2016c). Besides, the separated S2p peaks also showed bonds of S–C, C–S–C, S–O, and SO_4^{2-}, stemming from the H_2SO_4 treatment (Fig. S5). The surface-adhering SO_4^{2-} became shielded after the rigorous shaking during adsorption.

Furthermore, the N1s and O1s core-level spectra were deconvoluted as shown in Fig. S6 and S7. In the N1s spectra, the peaks at 399.27 and 400.66 eV represent the amino and peptide bonds emanating from the protein portion of the original biomass (Fig. S6(a)). The H_2SO_4-AC, however, presented different N-containing peaks assignable to pyridinic-N (397.57 eV), pyrrolic-N (399.07 eV), graphitic-N (400.46 eV), oxidized-N/–NH_2 (402.78 eV), and physisorbed/chemisorbed –N/N_2 (406.90 eV), suggesting that the AC lattices were doped with N atoms, possibly originating from the N_2 environment employed for the synthesis (Fig. S6(b)) (Lazar et al., 2019; Patel et al., 2015; Zhao et al., 2017). The doping process is systematic and may involve the sequential formation of five-membered pyrroles, which may undergo ring expansion into pyridines, and subsequently condense into graphitic-N (Arrigo et al., 2008; Grzyb et al., 2016; Patel et al., 2015). Interaction of the N-doped H_2SO_4-AC with Au led to peak shifts towards higher binding energy values, with a new nitro (–NO_2) peak emerging at 405.49 eV (Fig. S6(c)) (Liu et al., 2016). This is indicative of the involvement of the N groups in aiding the adsorption/reduction of Au(III) (Bediako, J. K.

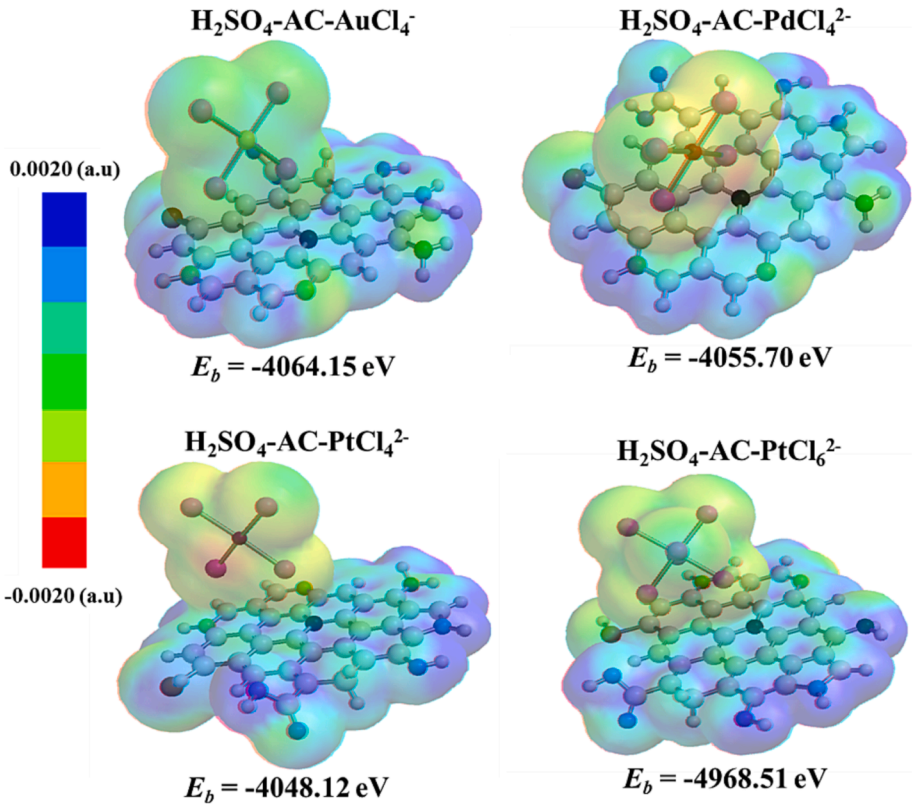

Fig. 5. Molecular electron potential (ESP) energy surfaces of the interaction between the optimized structure of H_2SO_4-AC and $AuCl_4^-$, $PdCl_4^{2-}$, $PtCl_4^{2-}$ and $PtCl_6^{2-}$ complexes.

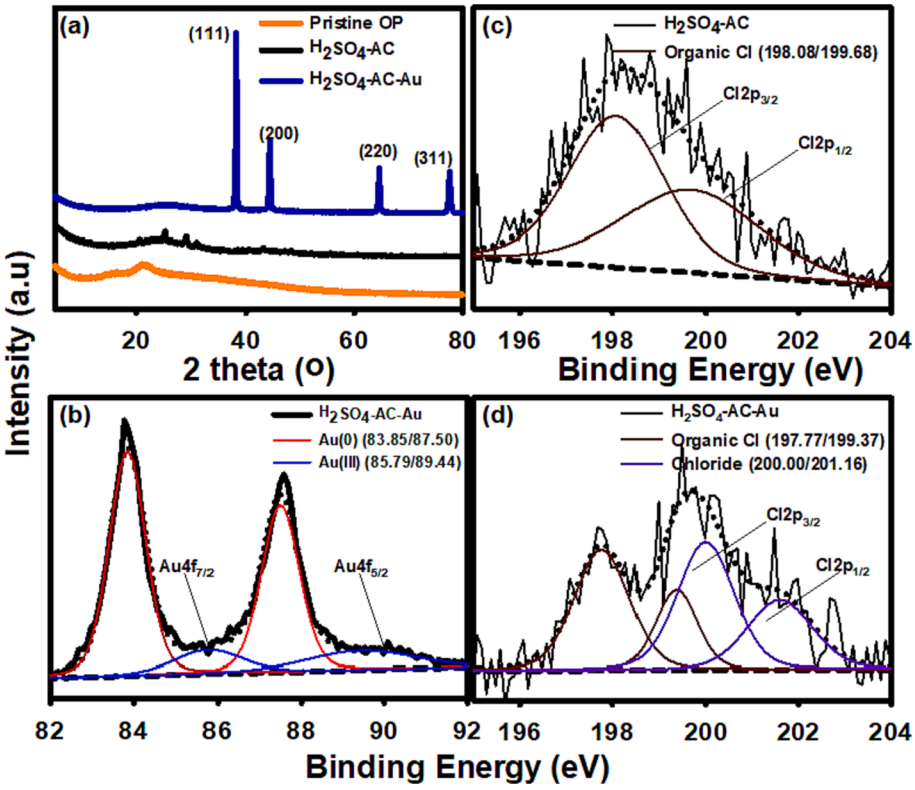

Fig. 6. Presentation of (a) XRD patterns and deconvoluted XPS spectra of (b) Au4f and (c) and (d) Cl2p for the pristine and activated carbon samples.

et al., 2020a; Lin et al., 2023).

Alternatively, the deconvoluted O1s spectrum of the pristine OP produced three characteristic peaks representative of adhering water molecules (H_2O, 533.57 eV), epoxy (C–O, 532.55 eV) and carbonyl (C = O, 531.65 eV) groups (Fig. S7(a)), whilst the H_2SO_4-AC displayed only epoxy and carbonyl groups (Fig. S7(b)) (Ganguly et al., 2011; Wagner, 1979). Notably, the total oxygen proportion of the H_2SO_4-AC increased significantly and a C–O/C = O ratio swing was observed after adsorption (Fig. S7(c)), indicating the simultaneous oxidation of the O-containing groups, e.g. OH to carbonyl (C = O) group, consequently contributing to the reduction of Au(III). Remarkably, a series of concurrent electron transfer cycles might have resulted in redox reactions leading to the reduction of Au (Bediako et al., 2020; Lin et al., 2023). Based on the evidences of Au(III) reduction to Au(0), the potential adsorption and reduction reactions are proposed in Eq. (8) – Eq. (10) (Wang et al., 2015; Wei et al., 2016c), and further illustrated schematically in Fig. 7. As discussed in the computational analysis, electrostatic interaction appeared to be favored by the deep-seated charged graphitic-N, whilst the edge-bound oxidized-N (NO), primary amine (NH_2) and hydroxyl (OH) groups induced the reduction of the Au(III) to Au(0).

$$\text{Ion-exchange/electrostatic interaction: } R\text{–}N^{+}Cl^{-} + AuCl_4^{-} \rightleftharpoons (R\text{–}N^{+})AuCl_4^{-} + Cl^{-} \quad (8)$$

$$\text{Reduction reaction (N): } R\text{–}NH_2 + 2AuCl_4^{-} + 2H_2O \rightarrow 2Au^{0} + R\text{–}NO_2 + 6H^{+} + 8Cl^{-} \quad (9)$$

$$\text{Reduction reaction (O): } 3R\text{–}OH + AuCl_4^{-} \rightarrow Au^{0} + 3(R = O) + 3H^{+} + 4Cl^{-} \quad (10)$$

3.4. Adsorption performance evaluation

To further assess the adsorption performance of the synthesized H_2SO_4-AC, adsorption isotherm, kinetics, and regeneration experiments were carried out. The resulting adsorption isotherm results were examined with the Langmuir and Freundlich isotherm models (Eq. (2) and (3)). Both models fitted the experimental data well; however, the Langmuir model offered a slightly better correlation than the Freundlich model, based on their coefficient of correlation, R^2 values (Fig. 8(a)). The Langmuir model which assumes monolayer adsorptions onto identical homogenous sites, estimated the maximum equilibrium uptake as 1679.74 ± 37.66 mg/g (Table S2). This uptake is comparatively higher than most adsorbents reported so far (Table S3). Although the initial slope was not as steep as would be normally expected, this is reasonably acceptable, especially for ACs, due to their mode of adsorption which involves diffusion of the adsorbates into the inner pores (Ahmed and Theydan, 2014; Bediako, J. K. et al., 2020b; Chen et al., 2013; Lazar et al., 2019).

The dimensionless constant, R_L given by Eq. (11) was derived from the Langmuir model, and used to provide additional information on the tendency of the adsorption process (Bediako, J. K. et al., 2016; Yan et al., 2012).

$$R_L = \frac{1}{1 + bC_0} \quad (11)$$

where C_0 is the initial adsorbate concentration (mg/L). The adsorption process can be described as either favorable ($0 < R_L < 1$), unfavorable ($R_L > 1$), linear ($R_L = 1$), or irreversible ($R_L = 0$) (Bediako, J. K. et al., 2016; Yan et al., 2012). Generally, smaller values of R_L ranging between 0 and 1 imply favorable adsorption with good binding affinity. The values obtain in this study were $0.2 < R_L < 0.9$ for the isotherm concentration range evaluated, reaffirming that the adsorption of Au onto the H_2SO_4-AC was favorable for the entire range of concentrations. This is presumably so, given that the pH_{pzc} of the H_2SO_4-AC is 6.8, implying that the surface of the AC is positively charged until the pH_{pzc}, which is conducive for effectively capturing the negatively charged precious metal complexes. The Freundlich model's n value of 1.95 ± 0.21 further asserts that the binding affinity was good and favorable, especially at higher initial concentrations (Yan et al., 2012).

Moreover, the kinetic experiment was conducted to establish the adsorption equilibrium rate. From Fig. 8(b), it could be observed that the adsorption equilibrium was attained within ca. 5 h. The kinetic curves rose sharply and steadily during the initial hours of contact between the H_2SO_4-AC and metal solution, allowing for more than 90 % of adsorption efficiency to be achieved only within the first 3 h. The kinetic data were correlated to the pseudo-first-order and pseudo-second-order models (Eq. (6) and (7)) to further investigate the adsorption process. Compared to the pseudo-first-order model, the pseudo-second-order model estimated the adsorption capacity very close to the experimental value (369.38 ± 13.07 vs. 371.99 ± 10.08), and the R^2 value of 0.99 was equally higher (Table S2). This suggests that the pseudo-second-order model adequately described the kinetic process of the present study (Park et al., 2018; Yan et al., 2012). Largely, the equilibrium rate could be described as adequate, considering the time-consuming cyclical redox reactions involved.

Noteworthily, it is inadequate to develop adsorbents that have high adsorption capacities but without potentials for regeneration, as this is crucial from economic and environmental perspectives (Dodson et al., 2015; Park et al., 2018). Therefore, 1 M concentration each of HNO_3, H_2SO_4, HCl, and a mixture of 0.5 M TU and 1 M HCl were evaluated for desorption and regeneration of the Au loaded-H_2SO_4-AC. As can be seen in Fig. 8c, the combination of TU and HCl led to nearly 100 % desorption efficiency in the first cycle, with only a subtle reduction even up to four cycles (Fig. 8d). The desorption using this mixture can result in the elution of both ionic and reduced forms of Au (Dwivedi et al., 2014; Bediako et al., 2020). In fact, acidified thiourea is known to be a strong complexing agent that is able to react with Au(0) and oxidize it to Au (III), according to Eq. (12) (Li et al., 2023; Dodson et al., 2015).

$$Au(0) + 2CS(NH_2)_2 = Au[\ CS(NH_2)2\ ]_2^{+} + e^{-} \quad (12)$$

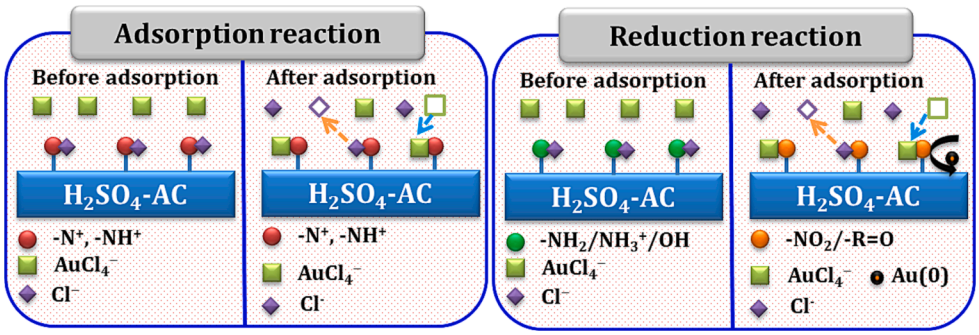

Fig. 7. Schematic illustration of the Au adsorption process by H_2SO_4-AC, leading to Au(III) adsorption and subsequent reduction to Au(0).

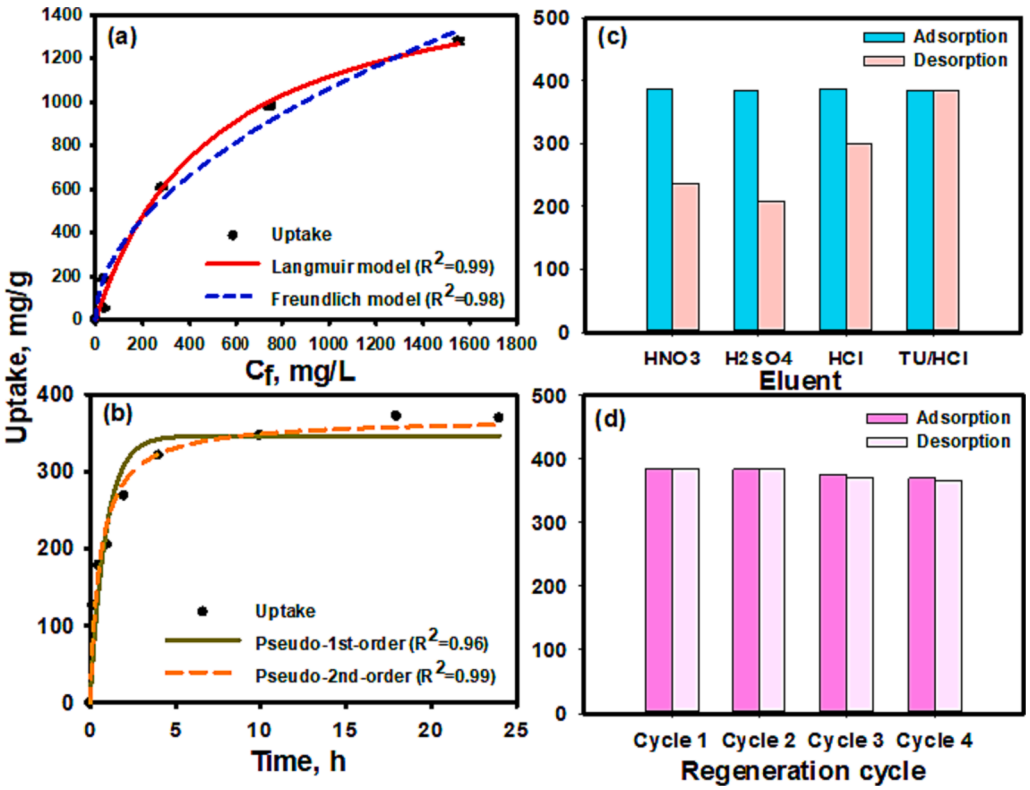

Fig. 8. Adsorption studies using H_2SO_4-AC. (a) isotherm curves (b) kinetics curves, (c) evaluation of different eluents, and (d) four cycles of successive adsorption-regeneration. Experimental conditions: adsorbent dosage; 0.02 g/30 mL (isotherm), 0.2 g/500 mL (kinetics), initial metal conc.; 0 – 2000 mg/L (isotherm), ~500 mg/L (kinetics and regeneration), temp.; 25 ± 2 °C, rotation speed; 140 rpm (isotherm and regeneration), 300 rpm (kinetics), reaction time; 24 h, pH; ~1.

Therefore, the TU-HCl mixture has been successful in leaching out the loaded Au metal likely because of the ability of acidified TU to complex both oxidized and reduced forms of Au. It can be remarked that the H_2SO_4-AC can be regenerated, making it potentially significant for practical application.

4. Conclusions

Activated carbons (ACs) were synthesized using different agro-waste biomass precursors and reagents for selective Au recovery from simulated acidic e-waste solutions. The Au selectivity and uptakes were evaluated through batch experiments, including adsorption isotherm, kinetics, and regeneration. The AC synthesized from OP and activated with H_2SO_4 exhibited the highest Au uptake. The Au selectivity was observed in the presence of interfering ions, and increased with increasing initial concentrations, i.e., from ~ 150 mg/L (low) to ~ 500 mg/L (high) in Au/Pt/Pd and Au/Pt/Pd/Ag/Co/Zn/Cu/Ni mixtures. The adsorption process was described to be dependent on concentration gradient, available binding sites and adsorption affinity. The maximum equilibrium uptake was 1679.74 ± 37.66 mg/g, according to the Langmuir model, and more than 90 % efficiency could be reached within 3 h. The increase in Au selectivity was spearheaded by ion exchange/electrostatic interactions and adsorption-reduction mechanisms as expounded through instrumental characterizations and DFT computations. Moreover, the loaded Au could be effectively eluted with a mixture of 0.5 TU and 1 M HCl to regenerate the spent AC up to at least four adsorption-regeneration cycles. Consequently, this work paves way for understanding the atomic and molecular level interactions leading to selective recovery of precious metals from complex mixtures. The study is also valuable for effectively tuning the capacity and selectivity of ACs towards Au through strategic treatment with H_2SO_4.

CRediT authorship contribution statement

John Kwame Bediako: Conceptualization, Formal analysis, Funding acquisition, Investigation, Methodology, Writing – original draft. **Enoch Kudoahor:** Formal analysis, Software, Validation, Writing – review & editing. **Che-Ryong Lim:** Data curation, Methodology, Software. **Nicole Sharon Affrifah:** Resources, Validation, Writing – review & editing. **Sok Kim:** Data curation, Formal analysis, Visualization. **Myung-Hee Song:** Funding acquisition, Resources. **Eveliina Repo:** Project administration, Supervision, Writing – review & editing.

Declaration of competing interest

The authors declare that they have no known competing financial interests or personal relationships that could have appeared to influence the work reported in this paper.

Data availability

Data will be made available on request.

Acknowledgements

Dr. Bediako expresses profound gratitude for the funding support from the European Union's Horizon 2020 research and innovation programme under the Marie Skłodowska-Curie grant agreement No. 101026202. Dr. Song also acknowledges funding support from the National Research Foundation (NRF) of Korea grant (2020R1C1C1006369).

Appendix A. Supplementary material

Supplementary data to this article can be found online at https://doi.

org/10.1016/j.wasman.2024.02.002.

References

Adams, C.R., Porter, C.P., Robshaw, T.J., Bezzina, J.P., Shields, V.R., Hides, A., Bruce, R., Ogden, M.D., 2020. An alternative to cyanide leaching of waste activated carbon ash for gold and silver recovery via synergistic dual-lixiviant treatment. J. Ind. Eng. Chem. 92, 120–130.

Ahmed, M.J., Theydan, S.K., 2014. Optimization of microwave preparation conditions for activated carbon from Albizia lebbeck seed pods for methylene blue dye adsorption. J. Anal. Appl. Pyrol. 105, 199–208.

Anirudhan, T.S., Fernandez, N.B., Mullassery, M.D., 2012. Removal of Cd(II) ions from aqueous solution using a cation exchanger derived from banana stem. J. Chem. Technol. Biotechnol. 87 (5), 714–722.

Arrigo, R., Havecker, M., Schlogl, R., Su, D.S., 2008. Dynamic surface rearrangement and thermal stability of nitrogen functional groups on carbon nanotubes. Chem. Commun. (Camb.) 40, 4891–4893.

Awual, M.R., Khaleque, M.A., Ferdows, M., Chowdhury, A.M.S., Yaita, T., 2013. Rapid recognition and recovery of gold(III) with functional ligand immobilized novel mesoporous adsorbent. Microchem. J. 110, 591–598.

Bacirhonde, P.M., Dzade, N.Y., Eya, H.I., Kim, C.S., Park, C.H., 2022. A potential peanut shell feedstock pyrolyzed biochar and iron-modified peanut shell biochars for heavy metal fixation in acid mine drainage. ACS Earth Space Chem. 6, 2651–2665.

Bediako, J.K., Wei, W., Kim, S., Yun, Y.-S., 2015. Removal of heavy metals from aqueous phases using chemically modified waste Lyocell fiber. J. Hazard. Mater. 299, 550–561.

Bediako, J.K., Kim, S., Wei, W., Yun, Y.S., 2016. Adsorptive separation of Pb(II) and Cu (II) from aqueous solutions using as-prepared carboxymethylated waste Lyocell fiber. Int. J. Env. Sci. Tec. 13 (3), 875–886.

Bediako, J.K., Wei, W., Yun, Y.-S., 2016. Conversion of waste textile cellulose fibers into heavy metal adsorbents. J. Ind. Eng. Chem. 43, 61–68.

Bediako, J.K., Song, M.-H., Yun, Y.-S., 2017. Fabrication and application of polyethylenimine/Ca-alginate blended hydrogel fibers as high-capacity adsorbents for recovery of gold from acidic solutions. Solid State Phenom. 262 (2017), 103–106.

Bediako, J.K., Park, S.W., Choi, J.-W., Song, M.-H., Yun, Y.-S., 2019. High-performance and acid-tolerant polyethylenimine-aminated polyvinyl chloride fibers: fabrication and application for recovery of platinum from acidic wastewaters. J. Environ. Chem. Eng. 7 (1), 102839.

Bediako, J.K., Lin, S., Sarkar, A.K., Zhao, Y., Choi, J.-W., Song, M.-H., Wei, W., Reddy, D. H.K., Cho, C.-W., Yun, Y.-S., 2020. Benignly-fabricated crosslinked polyethylenimine/calcium-alginate fibers as high-performance adsorbents for effective recovery of gold. J. Clean. Prod. 252.

Bediako, J.K., Choi, J.W., Song, M.H., Zhao, Y., Lin, S., Sarkar, A.K., Cho, C.W., Yun, Y.S., 2020a. Recovery of gold via adsorption-incineration techniques using banana peel and its derivatives: Selectivity and mechanisms. Waste Manage. 113, 225–235.

Bediako, J.K., Lin, S., Sarkar, A.K., Zhao, Y., Choi, J.W., Song, M.H., Cho, C.W., Yun, Y.S., 2020b. Evaluation of orange peel-derived activated carbons for treatment of dye-contaminated wastewater tailings. Environ. Sci. Pollut. Res. Int. 27 (1), 1053–1068.

Bediako, J.K., El Ouardi, Y., Massima Mouele, E.S., Mensah, B., Repo, E., 2023. Polyelectrolyte and polyelectrolyte complex-incorporated adsorbents in water and wastewater remediation - A review of recent advances. Chemosphere 325, 138418.

Bediako, J.K., Lim, C.-R., Repo, E., Choi, S.-H., Yun, Y.-S., 2023. Polyelectrolyte complex-derived adsorbents capable of selective recovery of precious metal from multiple mixtures. Chem. Eng. Sci. 274 (2023), 118688.

Bedin, K.C., Martins, A.C., Cazetta, A.L., Pezoti, O., Almeida, V.C., 2016. KOH-activated carbon prepared from sucrose spherical carbon: adsorption equilibrium, kinetic and thermodynamic studies for methylene blue removal. Chem. Eng. J. 286, 476–484.

Chand, R., Watari, T., Inoue, K., Kawakita, H., Luitel, H.N., Parajuli, D., Torikai, T., Yada, M., 2009. Selective adsorption of precious metals from hydrochloric acid solutions using porous carbon prepared from barley straw and rice husk. Miner. Eng. 22 (15), 1277–1282.

Changmei, S., Guanghua, Z., Chunhua, W., Rongjun, Q., Ying, Z., Quanyun, G., 2011. A resin with high adsorption selectivity for Au (III): Preparation, characterization and adsorption properties. Chem. Eng. J. 172 (2), 713–720.

Chen, Y., Zhai, S.-R., Liu, N., Song, Y., An, Q.-D., Song, X.-W., 2013. Dye removal of activated carbons prepared from NaOH-pretreated rice husks by low-temperature solution-processed carbonization and H_3PO_4 activation. Bioresour. Technol. 144, 401–409.

Chen, W., Zhang, H., Huang, Y., Wang, W., 2010. A fish scale based hierarchical lamellar porous carbon material obtained using a natural template for high performance electrochemical capacitors. J. Mater. Chem. 20 (23), 4773–4775.

Cortes, L.N., Tanabe, E.H., Bertuol, D.A., Dotto, G.L., 2015. Biosorption of gold from computer microprocessor leachate solutions using chitin. Waste Manage. 45, 272–279.

Din, M.I., Ashraf, S., Intisar, A., 2017. Comparative study of different activation treatments for the preparation of activated carbon: a mini-review. Sci. Prog. 100 (3), 299–312.

Dodson, J.R., Parker, H.L., Munoz Garcia, A., Hicken, A., Asemave, K., Farmer, T.J., He, H., Clark, J.H., Hunt, A.J., 2015. Bio-derived materials as a green route for precious & critical metal recovery and re-use. Green Chem. 17 (4), 1951–1965.

Dong, F., Wang, H., Sen, G., Wu, Z., Lee, S.C., 2011. Enhanced visible light photocatalytic activity of novel Pt/C-doped TiO_2/$PtCl_4$ three-component nanojunction system for degradation of toluene in air. J. Hazard. Mater. 187 (1–3), 509–516.

Dwivedi, A.D., Dubey, S.P., Hokkanen, S., Fallah, R.N., Sillanpää, M., 2014. Recovery of gold from aqueous solutions by taurine modified cellulose: An adsorptive–reduction pathway. Chem. Eng. J. 255, 97–106.

El Ouardi, Y., Virolainen, S., Massima Mouele, E.S., Laatikainen, M., Repo, E., Laatikainen, K., 2023. The recent progress of ion exchange for the separation of rare earths from secondary resources – A review. Hydrometall. 218.

Elwakeel, K.Z., El-Kousy, S., El-Shorbagy, H.G., El-Ghaffar, M.A.A., 2016. Comparison between the removal of reactive black 5 from aqueous solutions by 3-amino-1,2,4 triazole,5-thiol and melamine grafted chitosan prepared through four different routes. J. Env. Chem. Eng. 4 (1), 733–745.

Erim, Ü.C., Gülfen, M., Aydın, A.O., 2013. Separation of gold(III) ions by 1,8-diamino-naphthalene-formaldehyde chelating polymer. Hydrometall. 134, 87–95.

Freundlich, H.M.F., 1906. Über die Adsorption in Lösungen. Z. Phys. Chem. A 57, 385–470.

Fujiwara, K., Ramesh, A., Maki, T., Hasegawa, H., Ueda, K., 2007. Adsorption of platinum(IV), palladium(II) and gold(III) from aqueous solutions onto L-lysine modified crosslinked chitosan resin. J. Hazard. Mater. 146 (1–2), 39–50.

Ganguly, A., Sharma, S., Papakonstantinou, P., Hamilton, J., 2011. Probing the thermal deoxygenation of graphene oxide using high-resolution in situ X-ray-based spectroscopies. J. Phys. Chem. C 115 (34), 17009–17019.

Grzyb, B., Gryglewicz, S., Śliwak, A., Díez, N., Machnikowski, J., Gryglewicz, G., 2016. Guanidine, amitrole and imidazole as nitrogen dopants for the synthesis of N-graphenes. RSC Adv. 6 (19), 15782–15787.

Guidi, C.M., Mirri, C., Fratini, E., Licursi, V., Negri, R., Marcelli, A., Amendola, R., 2012. In vivo skin leptin modulation after 14 MeV neutron irradiation: a molecular and FT-IR spectroscopic study. Analyt. Bioanalyt. Chem. 404 (5), 1317–1326.

Gupta, V.K., Nayak, A., 2012. Cadmium removal and recovery from aqueous solutions by novel adsorbents prepared from orange peel and Fe_2O_3 nanoparticles. Chem. Eng. J. 180, 81–90.

Ho, Y.S., McKay, G., 1999. Pseudo-second order model for sorption processes. Process Biochem. 34, 451–465.

Huang, W., Zhang, H., Huang, Y., Wang, W., Wei, S., 2011. Hierarchical porous carbon obtained from animal bone and evaluation in electric double-layer capacitors. Carbon 49 (3), 838–843.

Iglesias, M., Anticó, E., Salvadó, V., 1999. Recovery of palladium(II) and gold(III) from diluted liquors using the resin duolite GT-73. Anal. Chim. Acta 381 (1), 61–67.

Kanmani, P., Rhim, J.-W., 2014. Physicochemical properties of gelatin/silver nanoparticle antimicrobial composite films. Food Chem. 148, 162–169.

Karaçetin, G., Sivrikaya, S., Imamoğlu, M., 2014. Adsorption of methylene blue from aqueous solutions by activated carbon prepared from hazelnut husk using zinc chloride. J. Anal. Appl. Pyrol. 110, 270–276.

Karhu, H., Kalantar, A., Väyrynen, I.J., Salmi, T., Murzin, D.Y., 2003. XPS analysis of chlorine residues in supported Pt and Pd catalysts with low metal loading. Appl. Catal. A: Gen. 247 (2), 283–294.

Khaled, A., El Nemr, A., El-Sikaily, A., Abdelwahab, O., 2009. Removal of Direct N Blue-106 from artificial textile dye effluent using activated carbon from orange peel: adsorption isotherm and kinetic studies. J. Hazard. Mater. 165 (1–3), 100–110.

Lagergren, S., 1898. Zur theorie der sogenannten adsorption gelöster stoffe. Kungl. Svensk. Vetensk. Handl. 24 (4), 1–39.

Lam, K.F., Yeung, K.L., McKay, G., 2006. An investigation of gold adsorption from a binary mixture with selective mesoporous silica adsorbents. J. Phys. Chem. B 110, 2187–2194.

Langmuir, I., 1918. The adsorption of gases on plane surfaces of glass, mica and platinum. J. Am. Chem. Soc. 40 (9), 1361–1403.

Lazar, P., Mach, R., Otyepka, M., 2019. Spectroscopic fingerprints of graphitic, pyrrolic, pyridinic, and chemisorbed nitrogen in N-doped graphene. J. Phys. Chem. C 123 (16), 10695–10702.

Le-Minh, N., Sivret, E.C., Shammay, A., Stuetz, R.M., 2018. Factors affecting the adsorption of gaseous environmental odors by activated carbon: A critical review. Crit. Rev. Environ. Sci. Technol. 48 (4), 341–375.

Li, K., Li, Q., Zhang, Y., Liu, X., Yang, Y., Jiang, T., 2023. Improved thiourea leaching of gold from a gold ore using additives. Hydrometall. 222, 106204.

Li, H., Wang, X., Cao, L., Zhang, X., Yang, C., 2015. Gold-recovery PVDF membrane functionalized with thiosemicarbazide. Chem. Eng. J. 280, 399–408.

Lin, S., Kumar Reddy, D.H., Bediako, J.K., Song, M.-H., Wei, W., Kim, J.-A., Yun, Y.-S., 2017. Effective adsorption of Pd(II), Pt(IV) and Au(III) by Zr(iv)-based metal–organic frameworks from strongly acidic solutions. J. Mater. Chem. A 5 (26), 13557–13564.

Lin, X., Song, M.-H., Tran, D.T., Lee, Y.-S., Yun, Y.-S., 2023. Development of polyethylenimine-functionalized cellulose fibers for recovery of Au(0) from Au(III)-containing acidic solutions through an adsorption–reduction–detachment–aggregation mechanism. J. Clean. Prod. 389, 136019.

Liu, J., Song, P., Ruan, M., Xu, W., 2016. Catalytic properties of graphitic and pyridinic nitrogen doped on carbon black for oxygen reduction reaction. Chinese J. Catalys. 37 (7), 1119–1126.

Mahapatra, D.M., Ramachandra, T.V., 2013. Algal biofuel: bountiful lipid from *Chlorococcum sp.* proliferating in municipal wastewater. Curr. Sci. 105 (1), 47–55.

Mao, J., Kim, S., Wu, X.H., Kwak, I.-S., Zhou, T., Yun, Y.-S., 2015. A sustainable cationic chitosan/E. coli fiber biosorbent for Pt(IV) removal and recovery in batch and column systems. Sep. Purif. Technol. 143, 32–39.

Martins, A.C., Pezoti, O., Cazetta, A.L., Bedin, K.C., Yamazaki, D.A.S., Bandoch, G.F.G., Asefa, T., Visentainer, J.V., Almeida, V.C., 2015. Removal of tetracycline by NaOH-activated carbon produced from macadamia nut shells: Kinetic and equilibrium studies. Chem. Eng. J. 260, 291–299.

Ouardi, Y.E., Aissouq, A.E., Chennah, A., Ouammou, A., Laatikainen, K., 2022. Synthesis, characterization, and DFT investigation of rhodamine B dye removal by activated carbon produced from argan nutshell. Biomass Convers. Biorefin. 1–12.
Park, S.W., Bediako, J.K., Song, M.-H., Choi, J.-W., Lee, H.-C., Yun, Y.-S., 2018. Facile fabrication of polyacrylic acid-polyvinyl chloride composite adsorbents for the treatment of cadmium-contaminated wastewater. J. Env. Chem. Eng. 6 (2), 2401–2408.
Park, S.-I., Kwak, I.S., Bae, M.A., Mao, J., Won, S.W., Han, D.H., Chung, Y.S., Yun, Y.-S., 2012. Recovery of gold as a type of porous fiber by using biosorption followed by incineration. Bioresour. Technol. 104, 208–214.
Park, S.-I., Kwak, I.S., Won, S.W., Yun, Y.-S., 2013. Glutaraldehyde-crosslinked chitosan beads for sorptive separation of Au(III) and Pd(II): opening a way to design reduction-coupled selectivity-tunable sorbents for separation of precious metals. J. Hazard. Meter. 248–249, 211–218.
Patel, M., Feng, W., Savaram, K., Khoshi, M.R., Huang, R., Sun, J., Rabie, E., Flach, C., Mendelsohn, R., Garfunkel, E., He, H., 2015. Microwave enabled one-pot, one-step fabrication and nitrogen doping of holey graphene oxide for catalytic applications. Small 11 (27), 3358–3368.
Qu, R., Sun, C., Wang, M., Ji, C., Xu, Q., Zhang, Y., Wang, C., Chen, H., Yin, P., 2009. Adsorption of Au(III) from aqueous solution using cotton fiber/chitosan composite adsorbents. Hydrometall. 100 (1–2), 65–71.
Ramesh, A., Hasegawa, H., Sugimoto, W., Maki, T., Ueda, K., 2008. Adsorption of gold (III), platinum(IV) and palladium(II) onto glycine modified crosslinked chitosan resin. Bioresour. Technol. 99 (9), 3801–3809.
Sarkar, A.K., Bediako, J.K., Choi, J.-W., Yun, Y.-S., 2019. Functionalized magnetic biopolymeric graphene oxide with outstanding performance in water purification. NPG Asia Mater. 11.
Shao, Y., Gan, Z., Epifanovsky, E., Gilbert, A.T., Wormit, M., Kussmann, J., Lange, A.W., Behn, A., Deng, J., Feng, X., 2015. Advances in molecular quantum chemistry contained in the Q-Chem 4 program package. Mol. Phys. 113 (2), 184–215.
Soleimani, M., Kaghazchi, T., 2008a. Activated hard shell of apricot stones: A promising adsorbent in gold recovery. Chinese J. Chem. Eng. 16 (1), 112–118.
Soleimani, M., Kaghazchi, T., 2008b. Adsorption of gold ions from industrial wastewater using activated carbon derived from hard shell of apricot stones – an agricultural waste. Bioresour. Technol. 99 (13), 5374–5383.
Song, M.-H., Harikishore Kumar Reddy, D., Yun, Y.-S., 2016. Fabrication of high performance amine-rich magnetic composite fibers for the recovery of precious Pt (iv) from acidic solutions. RSC Adv. 6(92), 89089-89097.
Unur, E., 2013. Functional nanoporous carbons from hydrothermally treated biomass for environmental purification. Micropor. Mesopor. Mat. 168, 92–101.
Wagner, C.D., 1979. Handbook of X-ray photoelectron spectroscopy: a reference book of standard data for use in X-ray photoelectron spectroscopy. Physical Electronics Division, Perkin-Elmer Corp.
Wang, F., Zhao, J., Zhu, M., Yu, J., Hu, Y.-S., Liu, H., 2015. Selective adsorption-deposition of gold nanoparticles onto monodispersed hydrothermal carbon spherules: a reduction-deposition coupled mechanism. J. Mater. Chem. A 3 (4), 1666–1674.
Wei, W., Kim, S., Song, M.-H., Bediako, J.K., Yun, Y.-S., 2015. Carboxymethyl cellulose fiber as a fast binding and biodegradable adsorbent of heavy metals. J. Taiwan Inst. Chem. Eng. 57, 104–110.
Wei, W., Cho, C.-W., Kim, S., Song, M.-H., Bediako, J.K., Yun, Y.-S., 2016a. Selective recovery of Au(III), Pt(IV), and Pd(II) from aqueous solutions by liquid–liquid extraction using ionic liquid Aliquat-336. J. Mol. Liq. 216, 18–24.
Wei, W., Lin, S., Reddy, D.H.K., Bediako, J.K., Yun, Y.-S., 2016b. Poly(styrenesulfonic acid)-impregnated alginate capsule for the selective sorption of Pd(II) from a Pt(IV)-Pd(II) binary solution. J. Hazard. Meter. 318, 79–89.
Wei, W., Reddy, D.H.K., Bediako, J.K., Yun, Y.-S., 2016c. Aliquat-336-impregnated alginate capsule as a green sorbent for selective recovery of gold from metal mixtures. Chem. Eng. J. 289, 413–422.
Won, S.W., Kotte, P., Wei, W., Lim, A., Yun, Y.-S., 2014. Biosorbents for recovery of precious metals. Bioresour. Technol. 160, 203–212.
Yan, H., Yang, L., Yang, Z., Yang, H., Li, A., Cheng, R., 2012. Preparation of chitosan/poly(acrylic acid) magnetic composite microspheres and applications in the removal of copper(II) ions from aqueous solutions. J. Hazard. Mater. 229–230, 371–380.
Yang, X., Wan, Y., Zheng, Y., He, F., Yu, Z., Huang, J., Wang, H., Ok, Y.S., Jiang, Y., Gao, B., 2019. Surface functional groups of carbon-based adsorbents and their roles in the removal of heavy metals from aqueous solutions: A critical review. Chem. Eng. J. 366, 608–621.
Zhang, J., Wang, X.X., Zhang, B., Ramakrishna, S., Yu, M., Ma, J.W., Long, Y.Z., 2018. In situ assembly of well-dispersed ag nanoparticles throughout electrospun alginate nanofibers for monitoring human breath-smart fabrics. ACS Appl. Mater. Interf. 10 (23), 19863–19870.
Zhao, X.H., Li, Q., Ma, X.M., Xiong, Z., Quan, F.Y., Xia, Y.Z., 2015. Alginate fibers embedded with silver nanoparticles as efficient catalysts for reduction of 4-nitrophenol. RSC Adv. 5 (61), 49534–49540.
Zhao, Y., Zhang, X., He, Y., Liu, N., Tan, T., Liang, C., 2017. Biomass derived nitrogen-doped highly porous carbon material with a hierarchical porous structure for high-performance lithium/sulfur batteries. Materials (Basel) 10 (10).
Zhou, N., Chen, H., Feng, Q., Yao, D., Chen, H., Wang, H., Zhou, Z., Li, H., Tian, Y., Lu, X., 2017. Effect of phosphoric acid on the surface properties and Pb(II) adsorption mechanisms of hydrochars prepared from fresh banana peels. J. Clean. Prod. 165, 221–230.